AD-A182 394 PREDICTION OF HIGH-SPEED ROTOR NOISE WITH A KIRCHHOFF FORMULA(U) ARMY AVIATION RESEARCH AND TECHNOLOGY ACTIVITY MOFFETT FIELD CA AEROFLIGHTDYNAMICS 1/1

UNCLASSIFIED DIRECTORATE T W PURCELL ET AL. 1987 F/G 20/1 NL

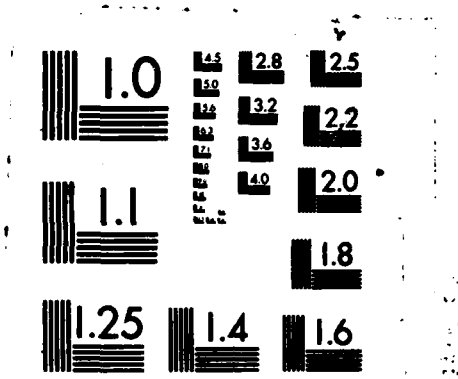

PREDICTION OF HIGH-SPEED ROTOR NOISE WITH A KIRCHHOFF FORMULA

Timothy W. Purcell, Roger C. Strawn, Yung H. Yu,

U.S. Army Aeroflightdynamics Directorate, AVSCOM
Ames Research Center, Moffett Field, California

1987

ABSTRACT

A new methodology has been developed to predict the impulsive noise generated by a transonic rotor blade. The formulation uses a full-potential finite-difference method to obtain the pressure field close to the blade. A Kirchhoff integral formulation is then used to extend these finite-difference results into the far-field. This Kirchhoff foumula is written in a blade-fixed coordinate system. It requires initial data across a plane at the sonic radius. This data is provided by the finite-difference solution. Acoustic pressure predictions show excellent agreement with hover experimental data for two hover cases of 0.88 and 0.90 tip Mach number. The latter of which has delocalized transonic flow. These results represent the first successful prediction technique for peak pressure amplitudes using a computational code.

LIST OF SYMBOLS

a_0 = atmospheric speed of sound, m/s

c = rotor chord length, m

h = nondimensional time step

I = identity matrix

J = Jacobian of coordinate transform matrix

M = hover tip Mach number

M_l = local Mach number

p = absolute pressure, N/m^2

P = nondimensional scaled disturbance pressure, $(p - p_0)/(\rho_0 a_0^2 \epsilon^{2/3})$

p_0 = atmospheric pressure, N/m^2

r = dimensional distance along the rotor in the spanwise direction, m

R = radial distance to the rotor tip, m

R_∞ = free stream subtraction term in Eqn. (5)

t = nondimensional time in nontransformed coordinate system

t' = dimensional time, s

T = scaled azimuthal angle location, $(1/\epsilon)(\theta + \beta - \tan^{-1}\beta)$

U = contravariant velocity normal to the η, ζ plane

V = contravariant velocity normal to the ξ, ζ plane

V_r = nondimensional scaled radial velocity component, $\phi_r/\omega R\epsilon$

W = contravariant velocity normal to the ξ, η plane

x, y, z = nondimensional coordinate system aligned with the blade

β = blade radial location, $[\left(\frac{\omega r}{a_0}\right)^2 - 1]^{1/2}$

$\hat{\beta}$ = $\rho^{2-\gamma}/J$

ϵ = inverse of the blade aspect ratio, c/R

γ = specific heat ratio

Γ = jump in potential across the wake normalized by $(a_0 c)$

ω = blade angular speed, rad/s

ϕ = dimensional velocity potential, m^2/s

Φ = non-dimensional velocity potential, ϕ/ca_0

ρ = fluid density normalized by free-stream values

$\hat{\rho}$ = ρ/J

ρ_0 = atmospheric density, kg/m^3

Presented at the AHS Specialists' Meeting on Aerodynamics and Aeroacoustics, Arlington, Texas, February 25-27, 1987.

σ = nondimensional integration variable, $-x$

τ = normalized time in the transformed coordinate system

θ = azimuthal angle in cylindrical coordinates relative to the blade

ξ, η, ς = transformed coordinate system

INTRODUCTION

Delocalization occurs for a high-speed rotor when the supersonic flow region at the blade tip connects to the farfield beyond the sonic cylinder. The sonic cylinder is the radial location beyond which the undisturbed flow appears to be supersonic to an observer on the blade. Flowfield nonlinearities are very significant at delocalization[1] and these nonlinearities cause large changes in the far-field acoustic levels.

Linear methods with monopoles and dipoles have consistently underpredicted the far-field acoustic levels for high tip Mach numbers. The methods developed by Ffowcs Williams and Hawkings[2] improve upon linear formulations by including the nonlinear quadrupole term in the acoustic pressure. Several methods have been developed for evaluating this quadrupole term[3-5], but difficulties concerning both the size of the quadrupole volume and the acquisition of aerodynamic data make this term difficult to integrate accurately. To date, neither computer codes nor experimental techniques have been able to successfully predict the far-field acoustic pressures associated with high-speed, delocalized rotor flows.

Computational fluid dynamics (CFD) computer codes in their non-approximated forms properly handle all flowfield non-linearities. Several computer codes exist for solving the three-dimensional full-potential equation for helicopter rotor flowfields.[6-10] Typically these codes are well developed for surface pressure and load predictions close to the blade. Far from the blade however, the grid densities are insufficient to resolve the details of the acoustic pressure field. Extending these codes to predict acoustics is too costly and perhaps impossible due to the huge grids required and instability problems that result from increasing the size of the computational domain. These instabilities occur as the radial distance away from the blade is increased, thereby increasing the freestream Mach number relative to the blade.[11]

The idea in this paper is to use a combined finite-difference code and Kirchhoff formulation in order to predict the acoustic far field. The finite-difference code used is FPR, which stands for Full-Potential Rotor code. It solves the fully conservative, three-dimensional, unsteady form of the full-potential eqauation and is described in Refs. 8 and 9. The FPR code is used to predict the pressure field both on the blade and along a plane located at the sonic radius. A computed solution at the sonic radius is well within the limits imposed by the maximum grid size and instability problems.

In extending this result to the far field, we use a Kirchhoff integral formulation that has been developed by Isom[12]. This Kirchhoff formulation uses integrals of the finite-difference results at the sonic cylinder to determine the acoustic pressures in the far field. It treats the linear sonic cylinder as a caustic where all the important data originates. This data is then propagated along linear characteristics to the far field.

The Kirchhoff formula uses non-rotating surface integrals of pressure and velocity. This non-rotating control surface should be large enough to enclose the rotor and the region of nonlinear flow. The linear sonic cylinder sufficiently encircles the nonlinear tip region. The flow field on the sonic cylinder comes from a numerical solution using a conservative full potential transonic code. This approach has several practical advantages. A large volume of quadrupole integral is replaced by a surface integral over the sonic cylinder surface. This control surface is a non-rotating one, eliminating mathematical singularities of the Ffowcs Williams and Hawkings equation. More importantly, the close proximity of the sonic cylinder to the rotor tip means that the finite-difference code only needs to solve the near-field region near the tip.

THE FULL-POTENTIAL ROTOR CODE

The Full-Potential Rotor solves the unsteady full-potential equation in strong conservation form. This equation is written below in generalized coordinates.

$$\frac{\partial}{\partial \tau}\left(\frac{\rho}{J}\right) + \frac{\partial}{\partial \xi}\left(\frac{\rho U}{J}\right) + \frac{\partial}{\partial \eta}\left(\frac{\rho V}{J}\right) + \frac{\partial}{\partial \varsigma}\left(\frac{\rho W}{J}\right) = 0 \quad (1)$$

with density given by:

$$\rho = \left\{1 + \frac{\gamma - 1}{2}\left[-2\Phi_\tau - (U + \xi_t)\Phi_\xi - (V + \eta_t)\Phi_\eta - (W + \varsigma_t)\Phi_\varsigma\right]\right\}^{\frac{1}{\gamma - 1}} \quad (2)$$

U, V and W are contravariant velocities given by

$$\begin{aligned} U &= \xi_t + A_1\Phi_\xi + A_4\Phi_\eta + A_5\Phi_\zeta \\ V &= \eta_t + A_4\Phi_\xi + A_2\Phi_\eta + A_6\Phi_\zeta \\ W &= \zeta_t + A_5\Phi_\xi + A_6\Phi_\eta + A_3\Phi_\zeta \end{aligned} \tag{3}$$

where

$$\begin{aligned} A_1 &= \xi_x^2 + \xi_y^2 + \xi_z^2 \\ A_2 &= \eta_x^2 + \eta_y^2 + \eta_z^2 \\ A_3 &= \zeta_x^2 + \zeta_y^2 + \zeta_z^2 \\ A_4 &= \xi_x\eta_x + \xi_y\eta_y + \xi_z\eta_z \\ A_5 &= \xi_x\zeta_x + \xi_y\zeta_y + \xi_z\zeta_z \\ A_6 &= \eta_x\zeta_x + \eta_y\zeta_y + \eta_z\zeta_z \end{aligned} \tag{4}$$

All velocities are normalised by a_∞, distances by the airfoil chord length, and time by the combination (c/a_∞). Density is normalised by the freestream value.

Equation (1) is solved by using first-order backward differencing in time and second-order central differencing in space. The temporal density derivative is locally linearised about the old time levels in a manner that preserves the conservative form. The resulting equation is approximately factored into ξ, η, and ζ operators. The steady-state version of this equation can be written as

$$\begin{aligned} &\left[I + hU^n\delta_\xi \pm Dh\tilde{\delta}_\xi - \frac{h^2}{\hat{\beta}^n}\delta_\xi(\beta A_1)^n\delta_\xi\right]\times \\ &\left[I + hV^n\delta_\eta - \frac{h^2}{\hat{\beta}^n}\delta_\eta(\beta A_2)^n\delta_\eta\right]\times \\ &\left[I + hW^n\delta_\zeta \pm Eh\tilde{\delta}_\zeta - \frac{h^2}{\hat{\beta}^n}\delta_\zeta(\beta A_3)^n\delta_\zeta\right](\Phi^{n+1} - \Phi^n) = \\ &\frac{h^2}{\hat{\beta}^n}\left[\delta_\xi(\beta U)^n + \delta_\eta(\beta V)^n + \delta_\zeta(\beta W)^n - R_\infty\right] \end{aligned} \tag{5}$$

where δ_ξ, δ_η, and δ_ζ represent central-difference operators in space. A steady state ADI relaxation algorithm solves this factored equation. The quantity R_∞ represents a numerical truncation error term caused by incomplete metric cancellation.

A sample grid for a rotor calculation is also shown in Fig. 1. An O-grid has been chosen for the basic finite-difference grid because of its efficient use of grid points. Rotor flows are computed by assigning an appropriate rotational coordinate velocity to each grid point. These coordinate velocities are given by ξ_t, η_t, and ζ_t. As a result, the rotor and the attached finite-difference grid move through still air and the velocity potential, Φ, is equal to zero in the far field.

Boundary conditions for the calculation are shown in Fig. 1. At the outer radial boundary of the O-grid, a non-reflection condition is used to prevent the accumulation of disturbances there. This boundary condition is described in Ref. 9. On the surface of the blade, a transpiration condition is used to simulate angle of attack conditions. Along the inner boundary plane, normal to the rotor, the spanwise contravariant velocity V, is set equal to η_t.

For lifting cases, the shed vorticity is specified as a jump in potential, Γ, imposed across the coordinate plane $\xi = 0$. This coordinate plane is approximately aligned with the shear layer from the trailing edge. Density is assumed to be continuous across the cut, and an unsteady transport equation for the potential jump is implemented in the wake.

The streamwise flux terms use upwind density biasing in regions of supercritical flow to ensure stability of the algorithm. The density is biased in both ζ and the ξ directions. The density always biases upwind no matter how the grid lines are oriented to the freestream.

If the finite-difference grid is extended radially beyond the sonic cylinder, then the freestream flow relative to the blade is supersonic and the full-potential equation becomes hyperbolic. The FPR code uses central-differencing in space with an upwind-biased artificial density in regions of supersonic flow. This method has been shown in Ref. 11 to give stability problems in regions where the freestream flow is supersonic.

In order to remedy these instabilities in the far field, the coefficients D and E have been added in the original FPR algorithm to act as stabilisers. The $\tilde{\delta}$ is a finite-difference operator chosen so that it always adds upwind data to the system. The parameters D and E control how much damping is added in the ξ and ζ directions respectively. The effect of these coefficients is to increase the diagonal dominance in the solution matrices. These terms approach zero as the solution converges to a steady-state result. This modification to the FPR code ensures a stable convergence at outer radial stations for cases where the freestream Mach number is well above one.

THE FAR-FIELD GEOMETRICAL ACOUSTICS FORMULATION

Numerical data for the potential in a region near the blade tip can be used in a geometrical acoustics approximation for pressure in the far field. This approximation will not be valid however, near the blade tip where the flowfield is non-linear and rapidly varying.

The geometrical acoustics approximation can be based on the small-disturbance potential equation. One form of this equation is

$$\frac{\phi_{t't'}}{a_0^2} - \nabla^2\phi = -\frac{\partial Q}{\partial t'} \tag{6}$$

The time-differentiated second order nonlinearity Q is given by

$$Q = \left(\frac{\gamma-1}{2a_0^4}\right)\phi_{t'}^2 + \frac{1}{a_0^2}|\nabla\phi|^2 \tag{7}$$

where γ is the ratio of specific heats and a_0 is the sound speed in undisturbed air. Note that Eqs. (6) and (7) assume that the local sound speed is constant. This is not the case however with the finite-difference solution close to the blade surface.

The objective is to use Eqn. (6) to find the disturbance pressure in the far field in terms of nonlinear initial data on some surface near the blade tip. This is accomplished by using a Kirchhoff solution to Eqn. (6) that converts it to an integral equation with Q as a source term. Next, a stationary phase approximation is applied that reduces the domain of all integrals to that of a data surface near the tip. This initial data surface is determined from the finite-difference code that solves the full-potential equation in the region close to the blade tip. The advantage of the geometrical acoustics approximation is that the finite-difference computation need not be continued from the blade surface all the way into the acoustic field.

With these ideas in mind, Eqn. (6) can be solved for the acoustic pressure at a point in the far field. Details of this solution are quite lengthy and will be described in Ref. 12. The resulting formula for acoustic pressure is given by

$$\begin{aligned} p(\beta,T) - p_0 = & \\ & -\frac{\rho_0 a_0^2 M^2 \epsilon^{4/3}}{(3)(6^{2/3})\pi\beta}\iint_A \frac{V_r(T,z)-V_r(\sigma,z)}{T-\sigma}\,\frac{d\sigma\,dz}{|T-\sigma|^{2/3}} \\ & +\frac{\rho_0 a_0^2 6^{2/3} M\epsilon^{4/3}}{36\pi\beta}\iint_A \frac{P(T,z)-P(\sigma,z)}{T-\sigma}\,\frac{sgn(T-\sigma)\,d\sigma\,dz}{|T-\sigma|^{1/3}} \\ & -\frac{\rho_0 a_0^2(\gamma+1)M\epsilon^{4/3}}{6\pi\beta}\iint_A \frac{P^2(T,z)-P^2(\sigma,z)}{T-\sigma}\,\frac{d\sigma\,dz}{T-\sigma} \end{aligned} \tag{8}$$

The location for the pressure evaluation is determined by the values of β and T, where β is a non-dimensional radial locatation and T is determined by the azimuthal angle relative to the blade. The use of Eqn. (8) is restricted to the plane of the rotor blade.

The surface integrals in Eqn. (8) are located at the sonic cylinder, ($r = a_0/\omega$). Choosing this location for initial data greatly simplifies the result. The integrals at this location are evaluated using the computed results from the FPR finite-difference calculation.

INTEGRATION OF THE FINITE-DIFFERENCE RESULTS

The FPR solution produces pressure data at the sonic cylinder on an O-grid plane of data perpendicular to the rotor axis. This solution is then interpolated onto a rectangular mesh for ease of integration. Since this plane does not lie on a constant radial station, a small approximation is introduced here which greatly simplifies the integration. The integrals then use the rectangular mesh data for input. A bi-cubic spline smooths the data between points on the mesh. A domain of ±3.5 chords in both the vertical and horizontal directions provides sufficient input for the integration.

All three integrals in Eqn. (8) contain singularities when T is equal to σ. In all three cases, the equations are integrated in the σ direction up to a small distance $\pm\epsilon$ from the singularity. The contributions at the singularity are computed separately. The functions inside the second and third integrals can be shown to be symmetric and odd at the singularity. Hence their integrated contributions are zero. The function inside the first integral is even, with a non-canceling contribution near the singularity. The value of this integral approaches the following limit at the singularity.

$$6\epsilon^{1/3} \int_{-\infty}^{\infty} \frac{\partial V_r(\sigma, z)}{\partial \sigma} \, dz$$

This singularity is not insignificant. It is usually the same order as the rest of the integral but of opposite sign. Near the pressure peak however, it suddenly switches sign and reinforces the rest of the integral value. At the pressure peak it contributes about 25% to the first integral.

Away from the pressure peak, the last two integrals are about the same magnitude as the first. At the peak however, the first two integrals may double in their respective values. The third integral, however, increases its value by almost two orders of magnitude, showing how important it is to the overall solution.

PREDICTION OF IMPULSIVE ROTOR NOISE

Our rotor-noise prediction scheme is demonstrated for two of the experimental test cases presented in Ref. 13. In this experiment, a 1/7 scale model of a UH-1H main rotor with a NACA 0012 airfoil section with a root-to-tip washout of 10.9°. This model was run at high-speed hover with thrust set to a low level in order to minimize the wake influence. Acoustic pressure data was measured in the plane of the rotor at a radial location equal to $3R$. A variety of hover tip Mach numbers were tested from $M = .8$ to $M = 1.0$

A top view of the finite-difference grid for the $M = .9$ computation is shown in Fig. 2. This figure shows a two-dimensional slice of the grid in the plane of the rotor. The blade tip is located at 13.7 chords in the spanwise direction. Only the outer three chords of the blade are computed in the FPR solution. A large number of grid planes are clustered in the far field in order to obtain good resolution of the acoustic pressures at the sonic cylinder ($r = 15.22$ chords). A total of 60 grid points were used in the chordwise direction, 38 in the spanwise direction, and 17 in the direction normal to the surface of the blade.

An untwisted, nonlifting NACA 0012 rotor blade was used for the acoustic prediction. This simplifies the finite-difference calculation because the rotor wake can be ignored. Boxwell et al.[13] have shown that thrust level is unimportant for high-speed impulsive noise cases. In general however, the FPR code can incorporate any of a number of rotor wake models.

Approximately 700 iteration steps were necessary to obtain a converged steady-state solution for this case. This represents approximately 10 minutes of CPU time on a Cray XMP 4/8 computer. The addition of the far-field damping terms causes this abnormally long run time. These damping terms are needed to control instabilities in regions where the freestream is supersonic. Typical iteration counts for the FPR code on conventional grids are about five times lower.

Computed Mach contours in the plane of the rotor for the $M = .9$ case are shown in Fig. 3. The local sonic Mach number contour, $M_l = 1$, deforms due to the local perturbation velocity field and touches the blade tip. The strong local shock on the tip portion of the rotor blade is now extended beyond the blade tip to the far field. This phenomenon is called delocalization. Delocalization causes a stong shock in far-field acoustic signatures at tip Mach numbers beyond the critical delocalization Mach number. The critical delocalization Mach number for this particular blade geometry is 0.9.

Figs. 4a and 4c show computed pressure distributions from the FPR code on the rotor plane at the sonic cylinder for the $M = .88$ and $M = .9$ cases respectively. Only the in-plane pressure distributions are shown in these plots although the solution is actually obtained across a plane at the sonic cylinder. These finite-difference predictions are then used as initial data for the Kirchoff integral formulation in Eq. (8) and the solution is carried to the far field.

The integrations in Eq. (8) require initial data over the entire sonic cylinder. The FPR solutions only provide this data ± 3.5 chords along the sonic cylinder in both the x and the z direction. Outside of this region, the pressures and radial velocities are assumed to be zero. This is clearly the case in the chordwise direction as shown in Figs. 4a and 4c. Here the pressure is seen to fall quickly to zero inside the chordwise computatinal domain for the FPR code. Peak pressure along the vertical axis along the sonic cylinder also falls rapidly to freestream values. This is demonstrated in Fig. 5 where the relative pressure has dropped to zero well within the ± 3.5 chord domain of the FPR code.

Figs. 4b and 4d compare computed far-field pressure results to experimental microphone measurements at the $r = 3R$ radial station. Good agreement is seen between the prediction and the data for peak pressure magnitudes and pressure pulse waveforms. For the $M = .88$ case (Fig. 4b) the computed result underpredicts the peak amplitude and shows a slightly wider pulse width compared to the experimental data. The symmetrical pulse shape agrees quite well with the data however.

The experimental data for the $M = .9$ case (Fig. 4d) show a strong shock in the pressure data that is not seen in the prediction. The prediction does show a steeper slope on the compression side however. This discrepency in the shock prediction may be attributed to two causes. First, the Kirchoff integral formulation has an assumption of constant sound propagation speed as shown in Eq. (8). The far-field nonlinear phenomenon may steepen the waveform as described by Isom[14]. If this is the case, then the Kirchoff integral formulation cannot be expected to model this.

A second cause for disagreement in the shock structure may be that the FPR finite-difference solution has smeared an existing shock at the sonic cylinder. Inadequate grid resolution could be the cause for this. If this is the case, then the resulting far-field pressure pulse will also show a smeared shock. In spite of these problems, the good agreement between experiment and computation appears to validate our new model for far-field rotor acoustic prediction techniques.

CONCLUSIONS

A new method has been developed to predict the impulsive noise signature generated by a high-speed transonic rotor blade. The matching of a finite-difference method and a Kirchhoff integral formula combines the advantages of each formulation in the regions where each is most appropriate. The finite-difference solution is used close to the blade, where flowfield nonlinearities are large. The Kirchhoff integral is used in the far field where its simplicity allows its application over a large domain.

Predictions with this method have shown excellent agreement with experimental data for two hover cases. One of these cases exhibits strongly delocalised flow. These results represent the first successful prediction technique for peak pressure amplitudes with a computational code.

REFERENCES

[1]Schmitz, F. H., and Yu, Y. H., "Transonic Rotor Noise—Theoretical and Experimental Comparisons," *Vertica*, Vol. 5, pp. 55–74, 1982.

[2]Ffowcs Williams, J. E., and Hawkings, D. L. "Sound Generation by Turbulence and Surfaces in Arbitrary Motion," Philos. Trans. R. Roc. London, Ser. A, vol. 264, pp. 321–342, May 8, 1969.

[3]Lowson, M.V., "Helicopter Noise: Analysis-Prediction and Methods of Prediction," *AGARD Lecture Series No. 63 on Helicopter Aerodynamics and Dynamics*, 1973.

[4]Schmitz, F. H., and Yu, Y. H., "Theoretical Modeling of High-speed Helicopter Impulsive Noise," *Journal of the American Helicopter Society*, Jan. 1979.

[5]Hawkings, D., "Noise Generation by Transonic Open Rotors," Westland Helicopters Limited, Research Paper 599, June 1979.

[6] Chang, I-Chung, and Tung, C., "Numerical Solution of the Full-Potential Equation for Rotors and Oblique Wings using a New Wake Model," AIAA Paper 85-0268, Jan. 1985.

[7]Sankar, N. L. and Prichard, D., "Solution of Transonic Flow Past Rotor Blades Using the Conservative Full-Potential Equation," AIAA Paper 85-5012 Oct. 1985.

[8] Strawn, R. C., and Caradonna, F. X.,"A Conservative Full-Potential Model for Unsteady Transonic Rotor Flows," *AIAA Journal* Vol. 25, No. 2, Feb. 1987, pp. 193-198.

[9]Strawn, R. C., and Tung, C., "The Prediction of Transonic Loading on Advancing Helicopter Rotors," *Presented at the AGARD/FDP Symposium on Applications of Computational Fluid Dynamics in Aeronautics*, April 7-10, 1986, Aix-en-Provence, France, (see also NASA TM-88238, April 1986).

[10]Egolf, T. A., and Sparks, S. P., "Hovering Rotor Airload Prediction Using a Full-Potential Flow Analysis with Realistic Wake Geometry," *Presented at the 41st Annual Forum of the American Helicopter Society*, Ft. Worth, Texas, 15-17 May, 1985.

[11]Purcell, T. W., "A Computational and Experimental Study of High-Speed Impulsive Noise from a Rotating Cylinder," AIAA paper 87-0253, Jan. 1987, see also Ph.D dissertation, Department of Aeronautics and Astronautics, Stanford University, June 1986.

[12]Isom, M., "Geometrical Acoustics and Transonic Helicopter Sound," U. S. Army Aeroflightdynamics Directorate, AVSCOM, Contract Technical Report, to be published May, 1987.

[13]Boxwell, D. A., Yu, Y. H., and Schmitz, F. H., "Hovering Impulsive Noise: Some Measured and Calculated Results," NASA CP-2052, 1978, and *Vertica*, Vol. 3, No. 1, 1979.

[14]Isom, M. P., "Acoustic Shock Waves Generated by a Transonic Helicopter Blade," *Presented at the 36th Annual National Forum of the American Helicopter Society*, Paper 63, May 1980.

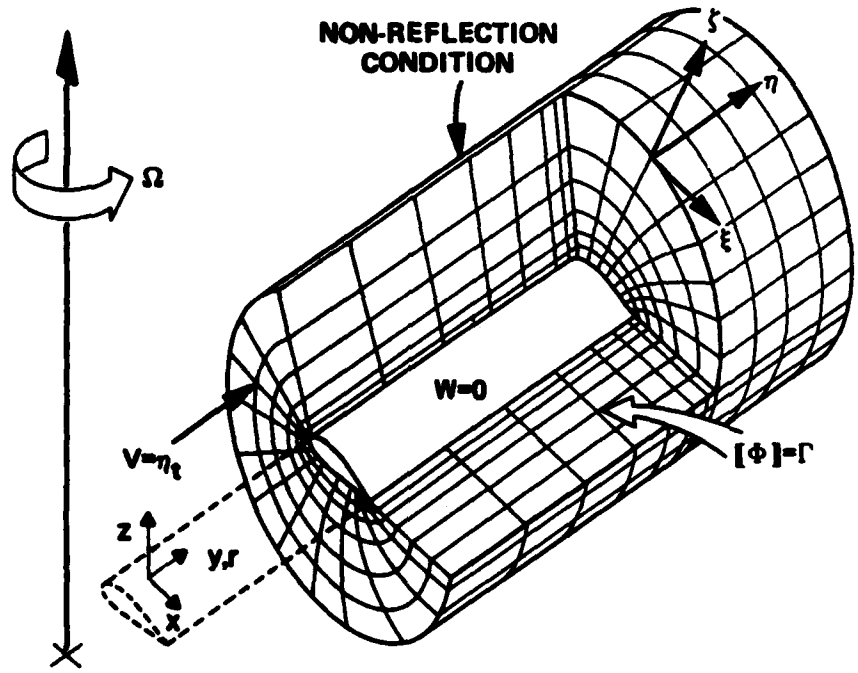

Fig. 1 Grid and boundary conditions for the FPR code.

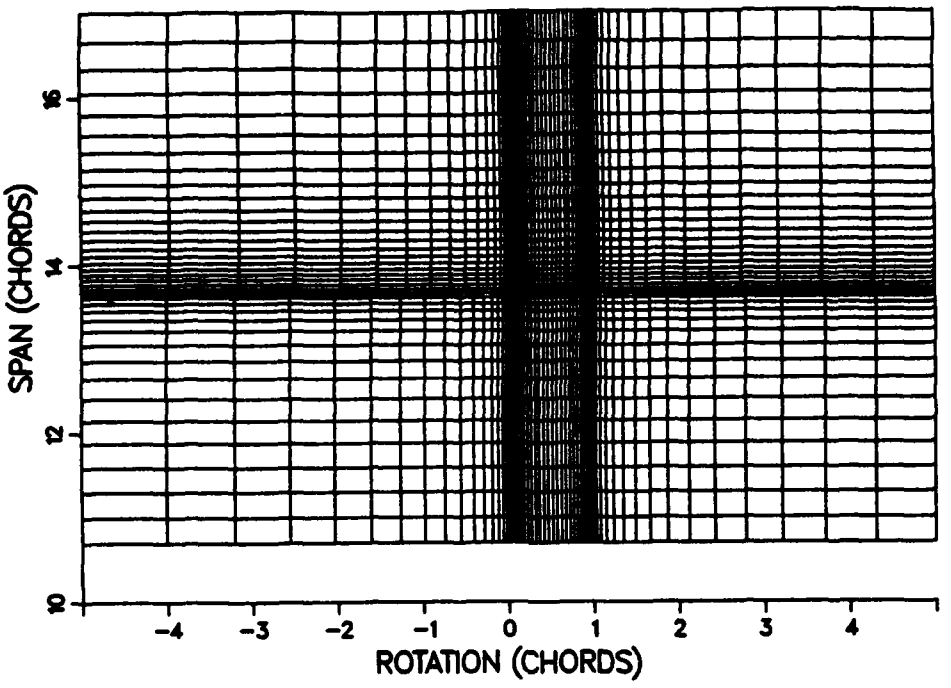

Fig. 2 Top view of the finite-difference grid for the $M = .9$ FPR calculation.

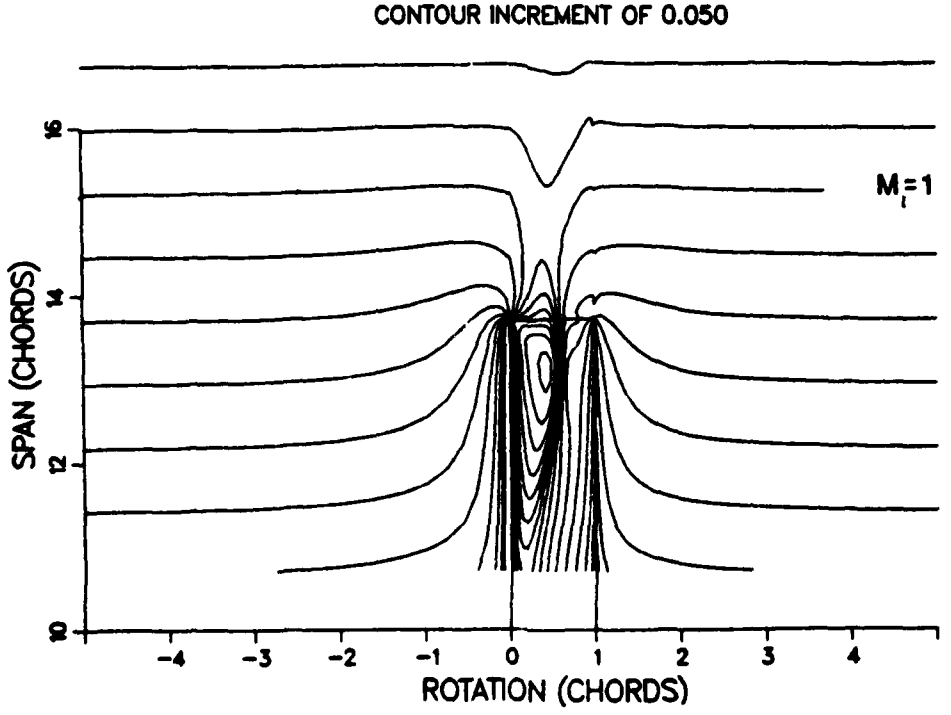

Fig. 3 Predicted Mach contours for the $M = .9$ hover case.

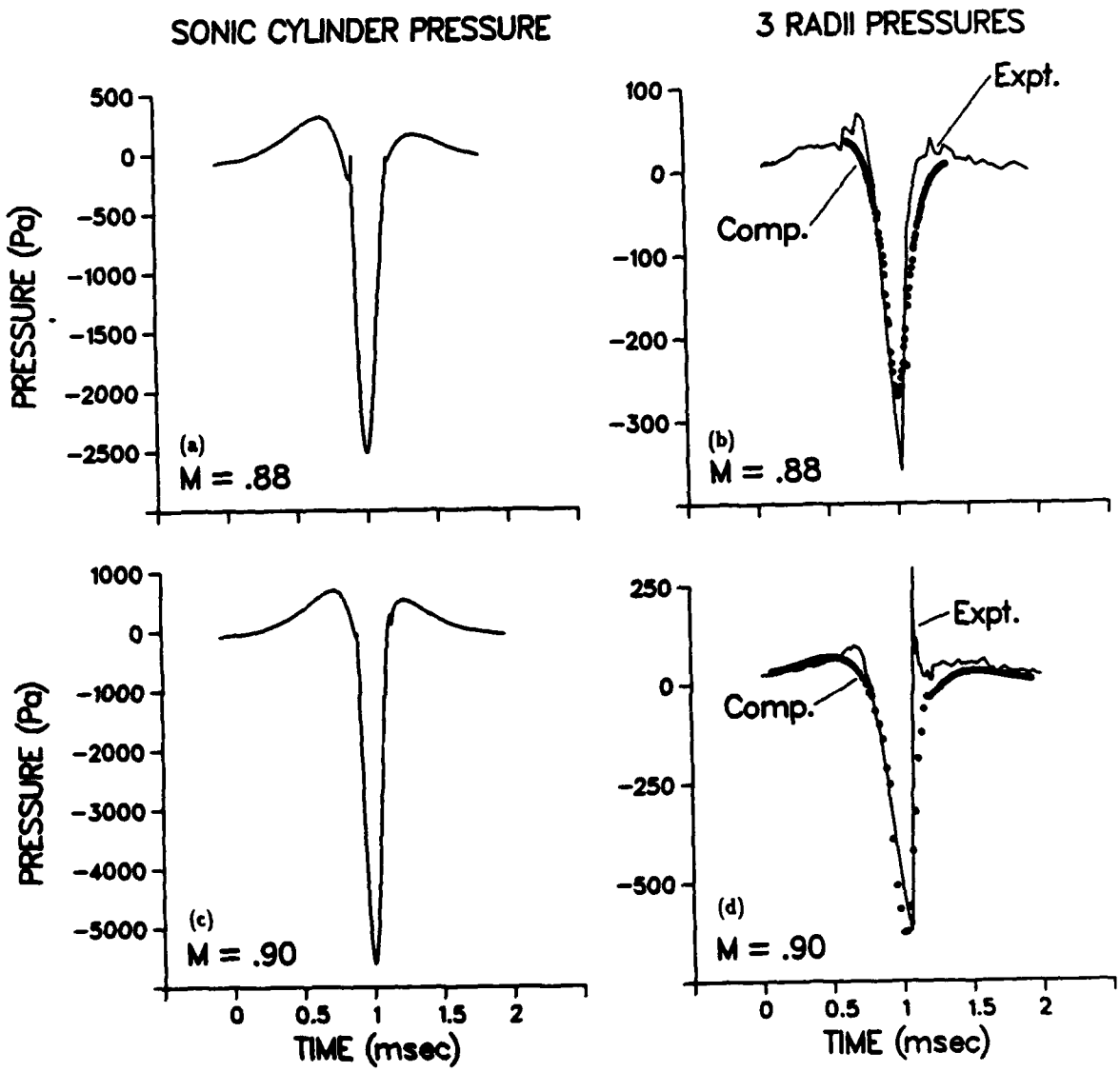

Fig. 4 Acousic pressure predictions for two hover tip Mach numbers, $M = .8$ and $M = .9$.

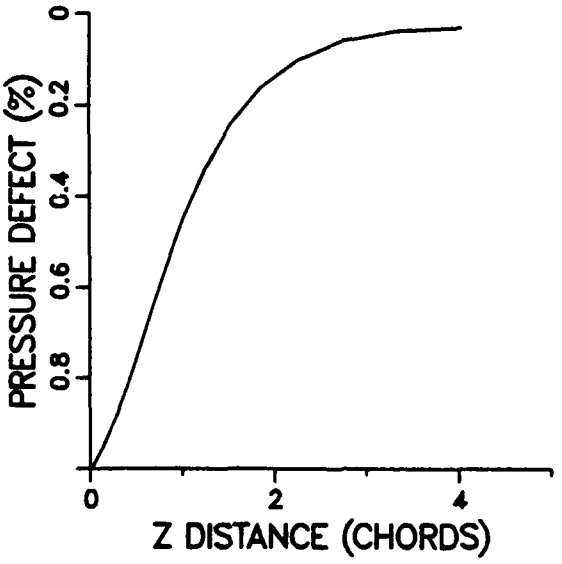

Fig. 5 Pressure prediction in the z direction. Pressure location is on the sonic cylinder at midchord.

END

8-87

DTIC